Assessment of proximal femur microarchitecture using ultra-high field MRI at 7 Tesla

Daphne Guenoun, Martine Pithioux, Jean-Christophe Souplet, Sandrine Guis, Thomas Le Corroller, Alexandre Fouré, Vanessa Pauly, J.P. Mattei, Monique Bernard, Maxime Guye, et al.

Version of Record: https://www.sciencedirect.com/science/article/pii/S2211568419301676
Manuscript_86b789b18c3b7e8f5f37d41edd580b81

Assessment of proximal femur microarchitecture using ultra-high field MRI at 7 Tesla

Short title:

Ultra-high field MRI of femur microarchitecture

Daphne Guenoun (1,2)*, Martine Pithioux (2), Jean-Christophe Souplet (3), Sandrine Guis (4), Thomas Le Corroller (1,2), Alexandre Fouré (3), Vanessa Pauly (5,6) , Jean-Pierre Mattei (4) , Monique Bernard (3) , Maxime Guye (3), Patrick Chabrand (2) , Pierre Champsaur (1,2), David Bendahan (3)

(1) APHM, Sainte-Marguerite Hospital, Institute for Locomotion, Department of Radiology, 13009 Marseille, France

(2) Aix Marseille Univ, CNRS, ISM, Inst Movement Sci, 13000 Marseille, France

(3) Aix Marseille Univ, CNRS, CRMBM UMR 7339, 13385, Marseille, France

(4) Department of Rheumatology, Aix-Marseille Université, CNRS, CRMBM UMR 7339, AP-HM, 13000 Marseille, France

(5) Aix Marseille Univ, Unité de recherche EA3279, Santé Publique et Maladies Chroniques: Qualité de vie concepts, usages et limites, déterminants, 13005 Marseille, France

(6) APHM, Service de Santé Publique et d'Information Médicale, Hôpital de la Conception, 13000 Marseille, France

***Corresponding author:** Daphne.guenoun@ap-hm.fr

Department of Radiology, APHM, Sainte-Marguerite Hospital, Institute for Locomotion,

13009, Marseille, France

Abstract

Purpose: The purpose of this study was to investigate bone microarchitecture of cadaveric proximal femurs using ultra-high field (UHF) 7-Tesla magnetic resonance imaging (MRI) and to compare the corresponding metrics with failure load assessed during mechanical compression test and areal bone mineral density (ABMD) measured using dual-energy X-ray absorptiometry.

Materials and methods: ABMD of ten proximal femurs from five cadavers (5 women; mean age= 86.2 ± 3.8 (SD) years; range : 82.5-90 years) were investigated using dual-energy X-ray absorptiometry and the bone volume fraction, trabecular thickness, trabecular spacing, fractal dimension, Euler characteristics, connectivity density and degree of anisotropy of each femur was quantified using UHF MRI. The whole set of specimens underwent mechanical compression tests to failure. The inter-rater reliability of microarchitecture characterization was assessed with the intraclass correlation coefficient (ICC). Associations were searched using correlation tests and multiple regression analysis.

Results: The inter-rater reliability for bone microarchitecture parameters measurement was good with ICC ranging from 0.80 and 0.91. ABMD and the whole set of microarchitecture metrics but connectivity density significantly correlated with failure load. Microarchitecture metrics correlated to each other but did not correlate with ABMD. Multiple regression analysis disclosed that the combination of microarchitecture metrics and ABMD improved the association with failure load.

Conclusion: Femur bone microarchitecture metrics quantified using UHF MRI significantly correlated with biomechanical parameters. The multimodal assessment of ABMD and trabecular bone microarchitecture using UHF MRI provides more information about fracture risk of femoral bone and might be of interest for future investigations of patients with undetected osteoporosis.

Keywords: Femur; Osteoporosis; Magnetic resonance imaging (MRI); Mineral bone density; 7 Tesla

Introduction

Fracture of the proximal femur is a major health burden in post-menopausal women and elderly persons. It represents the main source of osteoporosis-related mortality and morbidity [1]. Osteoporosis is an age-related progressive skeletal disease characterized by a reduced bone mass and microarchitectural alterations resulting in an increased bone fragility and susceptibility to fracture [2]. Bone strength is routinely evaluated from areal bone mineral density (ABMD) measurements using dual-energy X-ray absorptiometry (DXA) [3, 4]. Patients are commonly diagnosed as osteoporotic on the basis of the ABMD T-score [5, 6]. A score lower than 2.5 standard deviations (SDs) below the mean ABMD value quantified in a group of young control subjects (< 30 years) of the same gender and ethnicity is considered as outside the normal range [5, 6]. However, the diagnostic value of DXA-based ABMD has been recognized as limited for the prediction of fracture risk thereby indicating that ABMD would not allow bone microarchitecture assessment. Accordingly, low ABMD values would account for only 28% of hip fractures [7]. Similarly, a significant percentage of fractures has been reported in women with ABMD values above the accepted threshold [8-10]. While microarchitecture deterioration has actually been included in the definition of osteoporosis this aspect is not assessed using ABMD measurements [11]. Interestingly, bone microarchitecture can be assessed using high-resolution quantitative computed tomography (QCT) [12] but the corresponding tool is poorly available and has never been used for large groups of subjects [13].

Considering its non-radiating nature and the progress regarding radiofrequency coil technology and field strength, magnetic resonance imaging (MRI) of proximal femur microarchitecture has become possible [7, 14, 15]. It has been recently reported that post-menopausal women with a higher fracture risk can be distinguished from those with lower fracture risk on the basis of measurements obtained from ultra-high field (UHF) MRI [15]. On that basis, it has been suggested that UHF MRI can provide information about bone quality that are different and likely complementary than those provided by DXA. Although the very first results are promising, comparative analysis between MRI and biomechanical metrics are still very scarce with only one study performed at 1.5-T [14].

The purpose of this study was to investigate bone microarchitecture of cadaveric proximal femurs using UHF MRI and to compare the corresponding metrics with failure load assessed during mechanical compression tests and ABMD measured using DXA.

Materials and methods

Femoral specimens

Ten cadaveric proximal femora of 5 human donors (5 women; mean age, 86.2 ± 3.8 (SD) years; range: 82.5-90 years) were obtained within 10 days after death, according to the institutional safety and ethics regulations. Donor consent for research purposes was obtained prior to death. No information was available regarding the cause of death or previous diseases. Donors with scars in the region of proximal femur were excluded. All specimens were carefully cleaned of soft tissue and the femoral diaphysis was cut 10 cm below the lesser trochanter to facilitate bone attachment for mechanical testing. Specimens were stored at −20°C and progressively thawed at room temperature 6 hours before testing. A single defrosting cycle was required.

CT measurements

Each femur was scanned using a Light Speed® VCT 64 unit (General-Electric Healthcare) in order to detect femoral lesion (tumor) or fracture, and gas bubbles due to tissue degradation with the following parameters: field of view 12 cm; slice thickness, 0.625; interval, 0.625 mm; tube current, 365 mA; and tube potential, 120 KV.

DXA measurements

Specimens were positioned similarly to what is conventionally done for *in vivo* examination with a mild internal rotation. They were placed in a vessel filled with tap water up to 15 cm in height to simulate soft tissue [16]. DXA measurements were performed with a Prodigy® Scanner (General-Electric Healthcare). ABDM was measured in three regions of interest (ROIs) for each specimen (*i.e.,* femoral neck, intertrochanteric and greater trochanter regions). The total proximal ABDM was computed.

MRI

Each specimen was scanned using a 7-T whole-body MRI scanner (Siemens Healthineers) and a 28-channel proton coil. Once the initial MRI localized images were obtained for the three orthogonal planes, an interactive localized B_0 shimming was performed using the second-order shimming procedure provided by the manufacturer. High-resolution gradient recalled-echo images of each femur were acquired in the coronal plane using the following parameters: field of view, 140 × 140 mm²; acquisition matrix size, 832 × 832; contiguous slice thickness, 0.5 mm; TR/TE, 20/6 msec; flip angle, 15°; number of repetitions, 3; number of slices, 58; in-plane voxel size, 0.17 x 0.17 mm. The corresponding acquisition time was 37 min 36 s.

Each image was initially corrected for any remaining signal inhomogeneities using the N4 algorithm [17]. Using an open-source digital measurement software (ImageJ, NIH,) [18], images were binarized and thresholded as previously described [19]. For each slice, a 10 x 10 x 10 mm volume of interest (VOI) positioned at mid-distance between the top and the bottom of the greater trochanter was selected (*i.e.*, 60 x60 pixels in 20 slices) (Fig. 1). Bone volume fraction, trabecular thickness, trabecular spacing, fractal dimension, Euler characteristic, connectivity density and the degree of anisotropy were computed within the volume of interest (VOI) using BoneJ, which is an ImageJ module dedicated to bone images analysis.

Bone volume fraction corresponds to $\frac{Bone\ volume}{Total\ volume}$. Bone volume fraction is commonly related to porosity and has been considered as a surrogate of volumetric bone density rather than a strict measure of bone microarchitecture [20].

Fractal dimension is a bone texture parameter with the fractal dimension of bone-marrow surface giving some information on the degree of complexity or disorder of the bone microarchitecture. Fractal analysis expresses the roughness of the texture and characterizes the self-similarity of its gray-level variations over different scales [21]. Texture parameters have been reported as indirect indices of the three-dimensional microarchitecture [22].

The number of connected structures in a network can be determined from the Euler characteristic [23]. Trabecular bone can be considered as a network and its connectivity density can be calculated from the ratio between the connectivity estimate and the volume of the sample (~ number of trabeculae per unit volume) [18].

Anisotropy corresponds to the preferential spatial directional organization of a material. Trabecular bone is typically an anisotropic material with variable mechanical properties according to the direction of the applied strength, the maximum resistance being parallel to the main line of spans. The spans which first disappear in osteoporosis are the ones which undergo the least mechanical strengths [22]

Analyses were performed by two independent operators, a 7-year-experience skeletal radiologist (D.G.) and an engineer doctor specialized in MRI (J.C.S.).

Mechanical testing

Each specimen was loaded to failure in a universal testing machine (Instron 5566, Instron). Femur orientation within the loading apparatus was chosen so as to simulate a sideways fall on the greater trochanter [24, 25]. Specimens were fixed in resin (Epoxy Axon F23) at 15° internal rotation and the femoral shaft was oriented at 10° adduction within the apparatus. The load was applied to the greater trochanter through a pad, which simulated a soft tissue cover, and the femoral head was molded with resin to ensure force distribution over a greater surface area. The load was applied to the greater trochanter at a displacement rate of 10 mm/min. Failure load (in Newton) was defined as the first local maximum after which the load declined by more than 10%. Then, fractures were visually classified according to clinical criteria (femoral neck, intertrochanteric, subtrochanteric, or isolated greater trochanteric fractures) [26].

Statistical analysis

Each parameter was described using mean and standard deviation (SD), median and quartiles [Q1; Q3]. We firstly verified that the distribution of the parameters was not statistically different from the normal distribution using the Kolmogorov-Smirnov with exact *P*-value. The inter-rater reliability of microarchitecture characterization was assessed with the intraclass correlation coefficient (ICC) for each microarchitecture variable. The average coefficient of variation between rater was presented as CV. Then, we assessed the correlation between failure load and each of the parameters and between the parameters themselves using Pearson correlations coefficients (r) after having verified the linear relationship with scatter plots. The level of significance was set at $P < 0.05$.

To evaluate whether microarchitecture parameters combined to ABMD improved the accuracy of the model multivariate ridge regressions analyses (with femoral failure as the dependent factor) were performed. We used the coefficient of determination of the model (R^2) to compare quality of the model with ABDM alone (R^2) vs ABDM and different combinations of microarchitecture parameters (adjusted R^2 named adjR^2). The R^2 indicates the percentage of the variance in the dependent variable (the femoral failure) that the independent variables (microarchitecture parameters and ABDM) explain collectively. We first reported the R^2 of the univariate linear regression with ABDM as the only independent variables (R^2). Then, we reported the R^2 of the multivariate linear ridge regression with ABDM combined with one of the microarchitecture parameters adjusted (adjR^2). For each microarchitecture parameters, we measured the % of improvements of the R^2 using the following computation:

$$\frac{adjR^2 model\ with\ ABMD\ and\ one\ microarchitecure\ parameter - R^2 with\ ABMD\ only}{R^2 with\ ABMD\ only}.$$

The % of improvement measures to what extent the addition of each of microarchitecture parameters allows to better explain the variation of the femoral failure. The ridge regression was used to take account for co-linearity due to correlation between microarchitecture parameters.

Finally, a multivariate ridge regression analysis was performed with the whole set of microarchitecture parameters and ABMD as independent variables. We used a backward stepwise analysis (elimination one parameter after the other) to only include parameters significantly associated with femoral failure at the *P* value < 0.05. Statistical analyses were performed using SPSS V20 and ridge regression was performed using the SAS® software.

Results

The mean ABMD for the total hip was 0.72 ± 0.1 (SD) g/cm^2 (range: 0.62 - 0.86 g/cm^2). During the compression test, a fracture could be detected for a mean failure load of 1238.5 ± 507.4 (SD) N (range: 710.6 - 2113 N) (median =1034 N; Q1 = 809.6, Q3 = 1776.3). We observed one femoral neck and nine intertrochanteric fractures. No subtrochanteric or isolated greater trochanteric fracture was observed. Microarchitecture metrics are reported in Table 1 along with the corresponding descriptive statistics.

The ICCs for the microarchitecture measurements performed in the greater trochanter were 0.90 (CV = 6.2%) for bone volume fraction, 0.89 (CV = 6.6%) for trabecular thickness, and 0.80 (CV = 5.6%) for trabecular spacing, 0.81 (CV = 10.1%) for the degree of anisotropy, 0.88 (CV=9.5%) for connectivity density, 0.91 (CV = 4.7%) for fractal dimension and 0.88 (CV = 6.2%) for Euler characteristics.

All of the microarchitecture metrics but connectivity density significantly correlated with failure load and with each other (Table 1; Fig. 2). Bone volume fraction had the highest correlation with failure load ($r = 0.736$; $P = 0.01$) Most of the microarchitecture parameters strongly correlated with each other but only the degree of anisotropy correlated with trabecular thickness (Table 2). The connectivity parameters (*i.e.,* Euler characteristics and connectivity density) significantly correlated with each other ($P < 0.001$). Euler characteristics significantly correlated with load failure ($P=0.044$) whereas connectivity density did not ($P=0.063$).

Ridge regression analysis demonstrated that correlation with fracture load prediction could be significantly increased from $R^2=0.418$ to $adjR^2=0.69$ when bone microarchitecture parameters metrics were combined with ABMD (Table 3). More specifically, Euler characteristics was the variable with the largest influence on the R^2 increase when combined to ABMD: when ABMD was combined with Euler characteristics the $adjR^2$ yielded the value of 0.69 (improvement of 64.6%).When connectivity density was combined to ABMD, the $adjR^2$ yielded the value of 0.67 (60.3% of improvement); while fractal dimension was combined with ABMD, the $adjR^2$ yielded the value of 0.69 (62.9% of improvement). Similarly, improvement in failure load correlation was 54.3% when combining bone volume fraction and ABMD, 60.5% when combining trabecular spacing and ABMD, 22.2%when combining trabecular thickness and ABDM, and 7.6% when combining the degree of anisotropy and ABMD.

Using a ridge multivariate regression analysis including all the microarchitecture metrics and ABMD and after a backward elimination of the non-significant parameters (at alpha level equal to 0.05), fractal dimension was the single eliminated parameter.

Discussion

In the present study we assessed proximal femoral bone microarchitecture using UHF-MRI and compared the corresponding results with those from DXA and mechanical compression tests. The

correlations between bone microarchitecture parameters and mechanical compression tests were better than in those reported in further studies.

In our study, ABMD significantly correlated with failure load in line with two previous studies [16, 27]. The microarchitecture (bone volume fraction, trabecular thickness, trabecular spacing, the degree of anisotropy and Euler characteristics) and texture metrics (fractal dimension) also significantly correlated with bone strength in line with previous study [l5]. In addition, ABMD and microarchitecture metrics were not related thereby indicating, as previously suggested, that MRI and DXA provide different information regarding bone quality and fracture risk [15]. Interestingly, the statistical power of the correlation between the microarchitecture and the mechanical metrics was improved when both ABMD and a microarchitecture variable were combined further supporting that both indices are not providing similar information and that the combination can be of diagnostic interest [15].

Among the microarchitecture metrics, bone volume fraction displayed the largest correlation with failure load. These results further support those from previous MRI studies conducted in the distal radius, ankle, distal femur, wrist and vertebrae [14, 28, 29]. On the basis of 1.5-T MRI measurements (slice thickness = 300 µm, in plane resolution = 117 µm), Majumdar et al. reported a lower bone volume fraction in the distal radius of subjects with fragility fractures (mean bone volume fraction = 0.23) as compared to controls (mean bone volume fraction = 0.29) while Link et al. showed similar results in the calcaneal bone and in the proximal femur (mean bone volume fraction=0.33) [14, 28, 29]. In our population of women cadavers without femoral fractures, mean bone volume fraction at the proximal femur was slightly larger (*i.e.*, 0.37) and similar to the mean values reported by Chang et al. in women with fragility fractures [30]. In a study conducted at 3-T in 60 postmenopausal women, the authors did not report significant bone volume fraction difference between the control group and the group with osteoporotic fractures thereby illustrating that the higher resolution obtained at UHF might account for this apparently paradoxical result [15]. Link et al. found a significant correlation between bone volume fraction measured in the great trochanter and biomechanical testing in the femoral neck (r= 0.62) [14]. This correlation was validated when measurements were performed using 0.9 mm thickness MRI slices but not when thickness was reduced to 0.3 mm (r = 0.32) likely resulting from a reduced signal-to-noise ratio. In the present study, strong correlations were found between bone volume fraction and

other microarchitecture metrics suggesting a potential overlap between these variables for the assessment of bone quality.

Trabecular thickness and trabecular spacing were also very significantly correlated with failure load with correlation coefficient larger than those computed using ABMD values. This result supports those from previous studies, which have illustrated that trabecular volume and trabecular space both increased with age [31]. Combining trabecular spacing with ABMD significantly improved the failure load identification whereas combining trabecular thickness with ABMD did not, probably due to a lack of power of the study. Both Euler characteristic (64.8%) and connectivity density (60.3%) had a large impact on the fracture identification from the combination between microarchitecture metrics and ABMD thereby illustrating a great potential for the assessment of bone strength *in vivo* from combined measurements. One can be surprised by this result because connectivity density did not significantly correlate with failure load ($r = 0.606$; $P = 0.063$), maybe due to a lack of power of the study because p is close to significance. Nevertheless, in our study, connectivity density and ABDM did not correlate ($r = 0.145$; $P = 0.688$), they therefore provide different information on the failure load. And when adjusted on ABDM, connectivity density provides significant information on failure load.

In our study, the degree of anisotropy was significantly correlated with failure load in agreement with previous results indicating that anisotropy is one of the main accounting factors of the bone mechanical resistance [28]. Combining the degree of anisotropy and ABMD did not significantly improve the relationship between the microarchitecture and mechanical parameters in agreement to what has been previously suggested [28]. Indeed, in our study the degree of anisotropy and ABMD are significantly linked ($r = 0.637$; $P= 0.048$), that is why the degree of anisotropy does not provide any additional information on failure load vs. ABMD.

In the present study, fractal dimension was strongly correlated with both other microarchitecture metrics and failure load, and the failure load information was improved if fractal dimension was combined to ABMD. These results confirm those obtained from DXA measurements and using the trabecular bone score indicating that trabecular bone score combined with ABMD incrementally improved fracture assessment in postmenopausal women [32].

The VOIs used for the microarchitecture measurements were positioned in the greater trochanter according to previous results [15] and given the high image quality there. Gas

bubbles were present in the region of the femoral neck likely due to the metabolic processes occurring in *ex-vivo* specimen. Those gas bubbles generate important artifacts in MRI. A small VOI (1x1x1cm) similar as the recent study of Chang et al. was chosen in order to avoid bubbles. In addition, during the biomechanical tests, most of the femoral fractures occurred in the intertrochanteric region (only one in the femoral neck) [15]. Considering that our in-plane resolution was within the range of trabecular size, microstructure metrics could have been slightly biased due to partial volume effects. As previously indicated, the resolution we obtained might have caused artefactual widening of trabeculae. However, the correlative analyses with mechanical variables are still valid and of high interest. In addition, the resolution we obtained using UHF MRI (voxel size = 0.17 x 0.17 x 0.5mm) was almost equivalent to the resolution that can be achieved using HR-QCT [33] and similar to the resolution previously reported at 7-T [34]. Due to image blurring and X-ray exposure, HR-QCT cannot be used in clinical routine so that UHF MRI could be considered as an interesting alternative [12]. Acquisition time (37 min) was still too long for a clinical context but might be shortened using other MRI pulse sequences such as 3D fast spin-echo with out-of-slab cancellation [35].

Our study has some limitations. Our results have been obtained from a small number of specimens, although this number is similar to the amount used in some other studies [29]. Samples preparation including a freezing-defreezing process and soft tissue removal might have altered the cadaveric samples and biased the corresponding results. Considering that the range of ABMD values reported in the present study was similar to those previously published *ex-vivo* [16, 28,] this bias might be considered as minor. As hematopoietic bone marrow could be detected *in vivo*, one can wonder about a potential contamination of hematopoietic bone marrow for the signal processing [14]. In our old cadaveric specimens, active red marrow is not expected and corresponding hyperintensities were not observed.

In conclusion, the results of the present study demonstrate that microarchitecture metrics quantified from excised proximal femur using UHF MRI are correlated with biomechanical strength and could provide an additional assessment tool of bone quality. Combined with ABMD values, these parameters might improve the prediction of load failure in previously undetected osteoporotic patients.

Acknowledgment

This study was supported by the French IA Equipex 7T-AMI (2011) program *ANR-11-EQPX-0001* and the A*MIDEX 7T-AMISTART (2013) through the*ANR-11-IDEX-0001-02* program. The authors thank the *Assistance Publique des Hôpitaux de Marseille* (APHM), the *Centre National de la Recherche Scientifique* (CNRS UMR 7339) and *Aix-Marseille University* (AMU).

References

1- Cooper C, Campion G, Melton LJ. Hip fractures in the elderly: a world-wide projection. Osteoporos Int 1992;2: 285-9.

2- Consensus development conference: diagnosis, prophylaxis, and treatment of osteoporosis. Am J Med 1993 94: 646–50.

3- Cummings SR, Black DM, Nevitt MC, Browner W, Cauley J, Ensrud K, et al. Bone density at various sites for prediction of hip fractures. The Study of Osteoporotic Fractures Research Group. Lancet 1993;341: 72–5.

4- Cummings SR, Nevitt MC, Browner WS, Stone K, Fox KM, Ensrud KE, et al. Risk factors for hip fracture in white women. Study of Osteoporotic Fractures Research Group. N Engl J Med 1995;332: 767–73.

5- Kanis JA, Diagnosis of osteoporosis and assessment of fracture risk, Lancet 2002;359: 1929–36.

6- Marshall D, Johnell O, Wedel H, Meta-analysis of how well measures of bone mineral density predict occurrence of osteoporotic fractures. BMJ 1996;312: 1254–9.

7- Chang G, Deniz CM, Honig S, Egol K, Regatte RR, Zhu Y, et al. MRI of the hip at 7T: feasibility of bone microarchitecture, high-resolution cartilage, and clinical imaging. J Magn Reson Imaging 2014;39: 1384–93.

8- Cummings SR, Are patients with hip fractures more osteoporotic? Review of the evidence. Am J Med 1985;78: 487–94.

9- Schuit SCE, van der Klift M, Weel AEM, de Laet CEDH, Burger H, Seeman E, et al. Fracture incidence and association with bone mineral density in elderly men and women: the Rotterdam Study. Bone 2004;34: 195–202.

10- Wainwright SA, Marshall LM, Ensrud KE, Cauley JA, Black DM, Hillier TA, Study of osteoporotic fractures research Group. Hip fracture in women without osteoporosis. J Clin Endocrinol Metab 2005;90: 2787–93.

11- Link TM, Osteoporosis imaging: state of the art and advanced imaging. Radiology 2012;263: 3–17.

12- Lespessailles E, Chappard C, Bonnet N, Benhamou CL. Imaging techniques for evaluating bone microarchitecture. Joint Bone Spine 2006;73: 254–61.

13- Adams JE, Quantitative computed tomography. Eur J Radiol 2009; 71: 415–24.

14- Link TM, Vieth V, Langenberg R, Meier N, Lotter A, Newitt D, et al. Structure analysis of high resolution magnetic resonance imaging of the proximal femur: in vitro correlation with biomechanical strength and BMD. Calcif Tissue Int 2003;72: 156–65.

15- Chang G, Rajapakse CS, Chen C, Welbeck A, Egol K, Regatte RR, et al. 3-T MR Imaging of proximal femur microarchitecture in subjects with and without fragility fracture and nonosteoporotic proximal femur bone mineral density. Radiology 2018;287: 608–19.

16- Le Corroller T, Halgrin J, Pithioux M, Guenoun D, Chabrand P, Champsaur P. Combination of texture analysis and bone mineral density improves the prediction of fracture load in human femurs. Osteoporos Int 2012;23: 163–9.

17- Tustison NJ, Avants BB, Cook PA, Zheng Y, Egan A, Yushkevich PA, et al. N4ITK: improved N3 bias correction, IEEE Trans Med Imagin 2010;29: 1310–20.

18- Doube M, Kłosowski MM, Arganda-Carreras I, Cordelières FP, Dougherty RP, Jackson JS, et al. BoneJ: free and extensible bone image analysis in ImageJ. Bone 2010;47: 1076–9.

19- Prewitt JM, Mendelsohn ML, The analysis of cell images. Ann N Y Acad Sci 1966; 128: 1035–53.

20- Fields AJ, Eswaran SK, Jekir MG, Keaveny TM, Role of trabecular microarchitecture in whole-vertebral body biomechanical behavior. J Bone Miner Res 2009;24: 1523–30.

21- Brunet-Imbault B, Lemineur G, Chappard C, A new anisotropy index on trabecular bone radiographic images using the fast Fourier transform. BMC Med Imaging 2005;5: 4.

22- Pothuaud L, Benhamou CL, Porion P, Lespessailles E, Harba R, Levitz P, Fractal dimension of trabecular bone projection texture is related to three-dimensional microarchitecture. J Bone Miner Res 2000;15: 691–9.

23- Vasilić B, Rajapakse CS, Wehrli FW, Classification of trabeculae into three-dimensional rodlike and platelike structures via local inertial anisotropy. Med Phys 2009;36: 3280–91.

24- EEckstein F, Wunderer C, Boehm H, Kuhn V, Priemel M, Link TM, et al. Reproducibility and side differences of mechanical tests for determining the structural strength of the proximal femur. J Bone Miner Res 2004;19: 379–85.

25- Manske SL, Liu-Ambrose T, Cooper DML, Kontulainen S, Guy P, Forster BB, et al. Cortical and trabecular bone in the femoral neck both contribute to proximal femur failure load prediction. Osteoporos Int 2009;20: 445–53.

26- Zuckerman JD. Hip fracture, N Engl J Med 1996;334: 1519–25.

27- Seo SH, Lee J, Park IH, Efficacy of dual energy X-ray absorptiometry for evaluation of biomechanical properties: bone mineral density and actual bone strength. J Bone Metab 2014;21: 205–12.

28- Majumdar S, Link TM, Augat P, Lin JC, Newitt D, Lane NE, et al. Trabecular bone architecture in the distal radius using magnetic resonance imaging in subjects with fractures of the proximal femur. Osteoporos Int 1999;10: 231–9.

29- Link TM, Majumdar S, Augat P, Lin JC, Newitt D, Lu Y, et al. In vivo high resolution MRI of the calcaneus: differences in trabecular structure in osteoporosis patients. J Bone Miner Res 1998;13: 1175–82.

30- Chang G, Rajapakse CS, Regatte RR, Babb J, Saxena A, Belmont HM, et al. 3 Tesla MRI detects deterioration in proximal femur microarchitecture and strength in long-term glucocorticoid users compared with controls. J Magn Reson Imaging 2015;42: 1489-96.

31- Milovanovic P, Djonic D, Marshall RP, Hahn M, Nikolic S, Zivkovic V, et al. Micro-structural basis for particular vulnerability of the superolateral neck trabecular bone in the postmenopausal women with hip fractures. Bone 2012;50: 63–8.

32- Hans D, Goertzen AL, Krieg M-A, Leslie WD, Bone microarchitecture assessed by TBS predicts osteoporotic fractures independent of bone density: the Manitoba study. J Bone Miner Res 2011;26: 2762–9.

33- Sornay-Rendu E, Boutroy S, Munoz F, Delmas PD, Alterations of cortical and trabecular architecture are associated with fractures in postmenopausal women, partially independent of decreased BMD measured by DXA: the OFELY study. J Bone Miner Res 2007;22: 425–33.

34- Bhagat YA, Rajapakse CS, Magland JF, Magland JF, Love JH, Wright AC, et al. Performance of μMRI-Based virtual bone biopsy for structural and mechanical analysis at the distal tibia at 7T field strength. J Magn Reson Imaging 2011; 33:372–81.

35- Magland JF, Rajapakse CS, Wright AC, Acciavatti R, Wehrli FW, 3D fast spin echo with out-of-slab cancellation: a technique for high-resolution structural imaging of trabecular bone at 7 Tesla. Magn Reson Med 2010; 63:719–27.

Figure Legend

Figure 1: Typical magnetic resonance image in the coronal plane of a cadaveric femur in saline. A is the original image and B is the same image after bias correction. The white square indicates the volume of interest (VOI) location for further measurements, the VOI left top corner has been set to be in the middle of the axes defined by the top and bottom points of the greater trochanter. The corresponding image is shown in C. D and E are the images obtained after contrast enhancement and binarization.

Figure 2: Graph shows the relation observed between bone volume fraction (BVF) on abscissa and the femoral failure load (in Newton) on ordinate in 10 specimens.

Table 1. Mean, standard deviation (SD), quartile Q1 and Q3, median, for each imaging variable and Pearson correlation (r) between imaging variables and failure load.

Table 2. Pearson's correlation coefficient between areal bone mineral density and vertebral microarchitecture parameters.

Table 3. Multiple regression analysis of combinations of areal bone mineral density and microarchitecture parameters used to explain the femoral failure load.

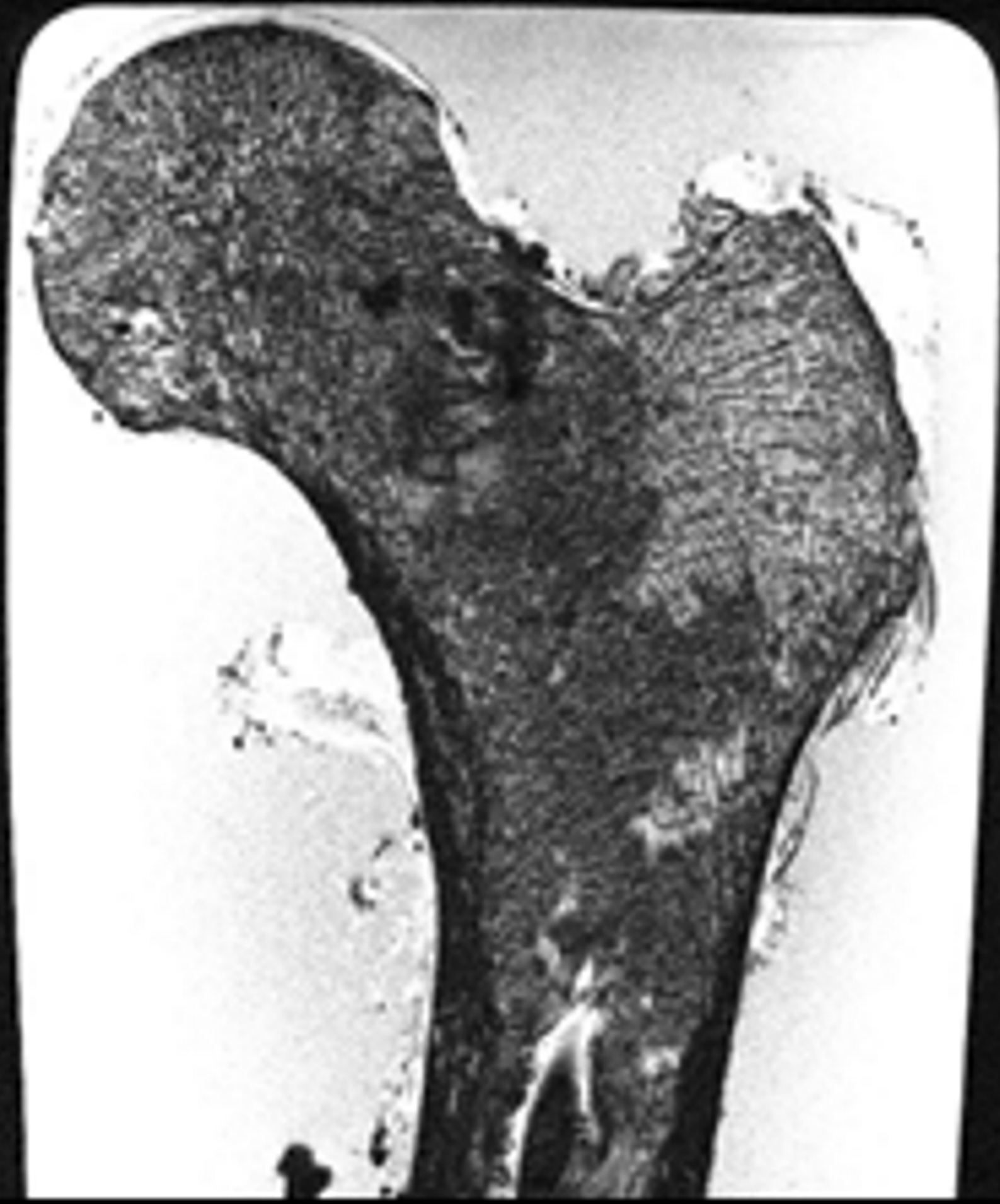

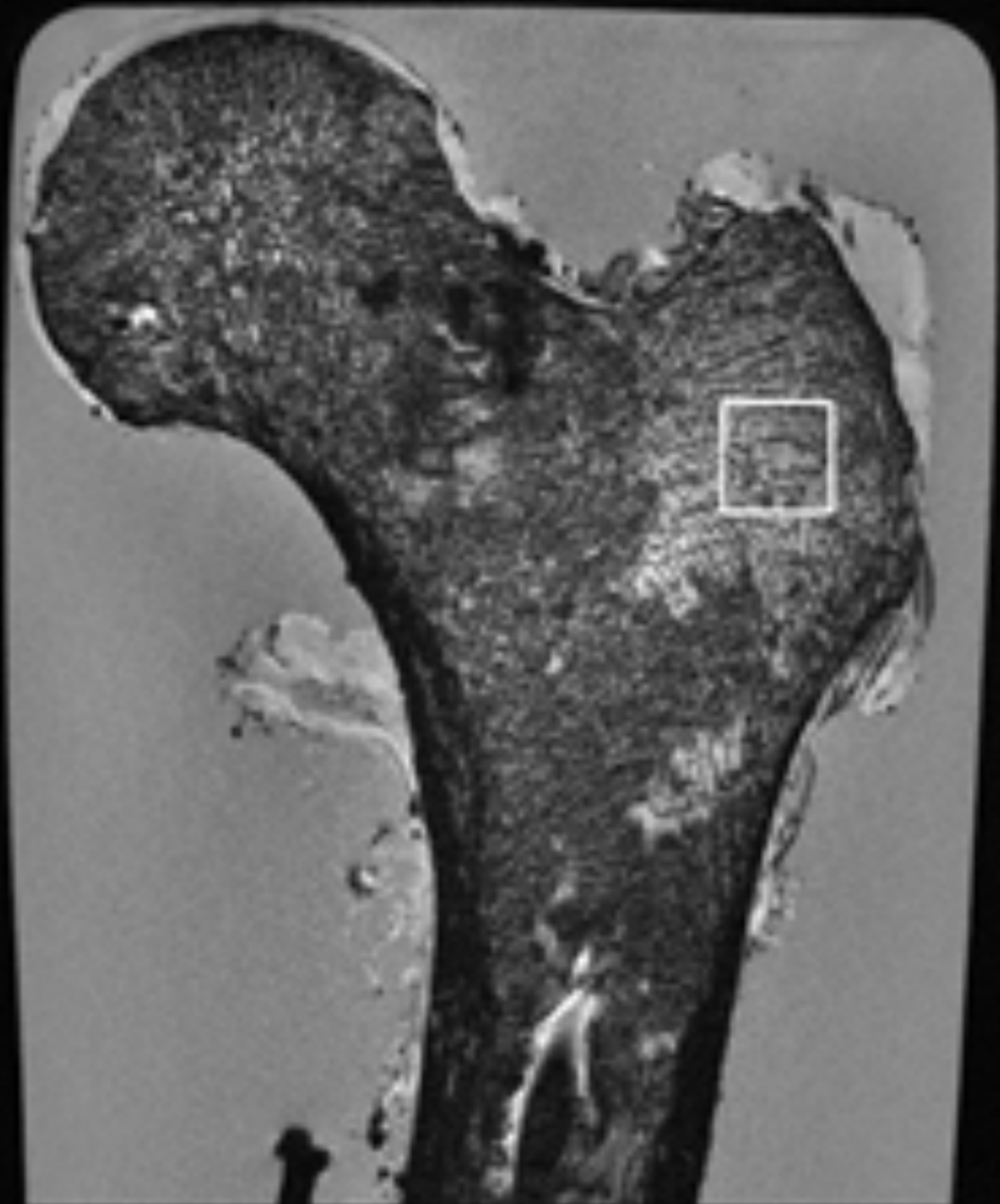

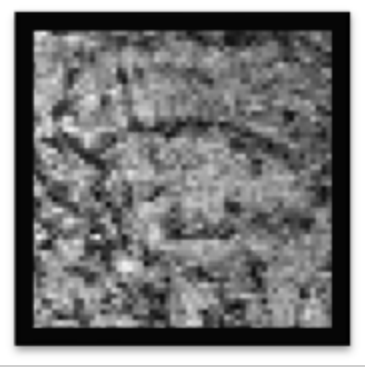

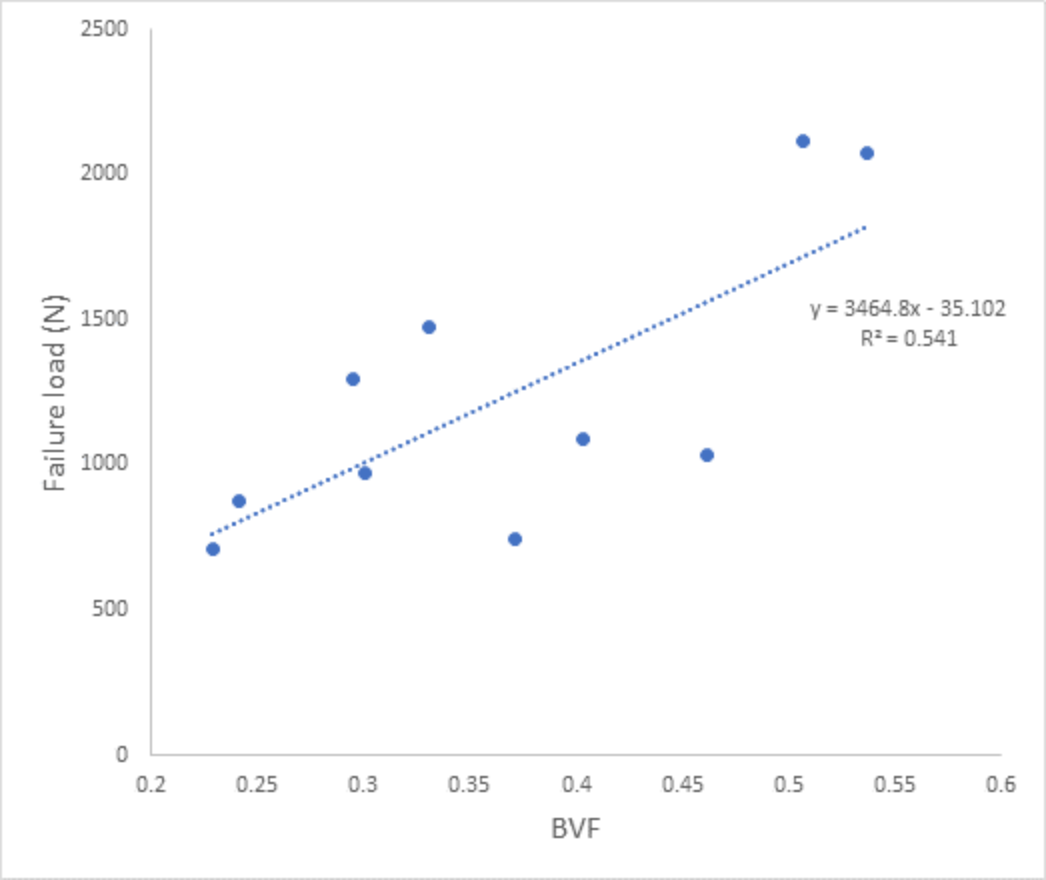
2500
2000
1500
1000
500
0
Failure load (N)
0.2
0.25
0.3
0.35
0.4
0.45
0.5
0.55
0.6
BVF
y = 3464.8x - 35.102
R² = 0.541

Table 1. Mean, standard deviation (SD), quartile Q1 and Q3, median, for each imaging variable and Pearson correlation (r) between imaging variables and failure load

Independent variable	**Mean**	**SD**	**Q1**	**Median**	**Q3**	**Pearson correlation r**	***P***
ABMD (g/cm²)	0.179	0.103	0.658	0.731	0.811	0.695	0.026
BVF	0.378	0.108	0.268	0.331	0.484	0.736	0.010
TT (mm)	0.329	0.028	0.304	0.316	0.354	0.706	0.022
TS (mm)	0.619	0.193	0.410	0.643	0.815	-0.699	0.025
FD	2.849	0.092	2.751	2.853	2.938	0.631	0.050
EC	-2336	744	-2847	-2358	-1540	-0.645	0.044
CD (mm³)	2.233	0.606	1.603	2.330	2.592	0.606	0.063
DA	0.663	0.034	0.643	0.669	0.687	0.677	0.031

ABMD indicates areal bone mineral density; BVF indicates bone volume fraction; TT indicates trabecular thickness; TS indicates trabecular spacing; FD indicates fractal dimension; EC indicates Euler characteristics; CD indicates connectivity density; aDA indicates degree of anistropy

	TT	TS	FD	EC	CD	DA	ABMD
BVF	0.926	-0.970	0.936	-0.908	0.872	0.662	0.417
P	*<0.001*	*< 0.001*	*< 0.001*	*< 0.001*	*0.001*	*0.037*	*0.231*
TT		-0.833	0.795	-0.709	0.655	0.638	0.585
P		*0.003*	*0.006*	*0.022*	*0.040*	*0.047*	*0.075*
TS			-0.955	0.943	-0.928	-0.695	-0.306
P			*< 0.001*	*<0.001*	*0.000*	*0.026*	*0.390*
FD				-0.963	0.944	0.546	0.171
P				*< 0.001*	*0.000*	*0.103*	*0.637*
EC					-0.993	-0.527	-0.188
P					*< 0.001*	*0.118*	*0.603*
CD						0.495	0.145
P						*0.146*	0.688

ABMD indicates areal bone mineral density; BVF indicates bone volume fraction; TT indicates trabecular thickness; TS indicates trabecular spacing; FD indicates fractal dimension; EC indicates Euler characteristics; CD indicates connectivity density and DA indicates degree of anisotropy. *P* indicates *P value*

Table 3. Multiple regression analysis of combinations of areal bone mineral density and microarchitecture parameters used to explain the femoral failure load

	ABMD	ABMD + BVF	ABMD + TT	ABMD + TS	ABMD + FD	ABMD + EC	ABMD + CD	ABMD + DA
R^2	0.418							
Ajusted R^2		0.645*	0.511	0.671*	0.684*	0.688*	0.670*	0.450
P	0.0256	0.0430	0.1576	0.0320	0.0275	0.0259	0.0323	0.256

ABMD indicates areal bone mineral density; BVF indicates bone volume fraction; TT indicates trabecular thickness; TS indicates trabecular spacing; FD indicates fractal dimension; EC indicates Euler characteristics; CD indicates connectivity density; DA indicates degree of anisotropy. *P* indicates the *P value* of the microarchitectural parameter in the multivariate ridge regression analysis. *Significant difference between adjusted R^2 of ABMD alone and ABMD + microarchitecture parameters